Pulmonary Surfactant Model Systems Catch the Specific Interaction of an Amphiphilic Peptide with Anionic Phospholipid

Hiromichi Nakahara,[†] Sannamu Lee,[‡] and Osamu Shibata[†*]
[†]Department of Biophysical Chemistry, Faculty of Pharmaceutical Sciences, Nagasaki International University, Nagasaki, Japan; and [‡]Department of Chemistry, Faculty of Science, Fukuoka University, Fukuoka, Japan

ABSTRACT Interfacial behavior was studied in pulmonary surfactant model systems containing an amphiphilic α-helical peptide (Hel 13-5), which consists of 13 hydrophobic and five hydrophilic amino acid residues. Fully saturated phospholipids of dipalmitoylphosphatidylcholine (DPPC) and dipalmitoylphosphatidylglycerol (DPPG) were utilized to understand specific interactions between anionic DPPG and cationic Hel 13-5 for pulmonary functions. Surface pressure (π)-molecular area (A) and surface potential (ΔV)-A isotherms of DPPG/Hel 13-5 and DPPC/DPPG (4:1, mol/mol)/Hel 13-5 preparations were measured to obtain basic information on the phase behavior under compression and expansion processes. The interaction leads to a variation in squeeze-out surface pressures against a mole fraction of Hel 13-5, where Hel 13-5 is eliminated from the surface on compression. The phase behavior was visualized by means of Brewster angle microscopy, fluorescence microscopy, and atomic force microscopy. At low surface pressures, the formation of differently ordered domains in size and shape is induced by electrostatic interactions. The domains independently grow upon compression to high surface pressures, especially in the DPPG/Hel 13-5 system. Under the further compression process, protrusion masses are formed in AFM images in the vicinity of squeeze-out pressures. The protrusion masses, which are attributed to the squeezed-out Hel 13-5, grow larger in lateral size with increasing DPPG content in phospholipid compositions. During subsequent expansion up to 35 mN m^{-1}, the protrusions retain their height and lateral diameter for the DPPG/Hel 13-5 system, whereas the protrusions become smaller for the DPPC/Hel 13-5 and DPPC/DPPG/Hel 13-5 systems due to a reentrance of the ejected Hel 13-5 into the surface. In this work we detected for the first time, to our knowledge, a remarkably large hysteresis loop for cyclic ΔV-A isotherms of the binary DPPG/Hel 13-5 preparation. This exciting phenomenon suggests that the specific interaction triggers two completely independent processes for Hel 13-5 during repeated compression and expansion: 1), squeezing-out into the subsolution; and 2), and close packing as a monolayer with DPPG at the interface. These characteristic processes are also strongly supported by atomic force microscopy observations. The data presented here provide complementary information on the mechanism and importance of the specific interaction between the phosphatidylglycerol headgroup and the polarized moiety of native surfactant protein B for biophysical functions of pulmonary surfactants.

INTRODUCTION

Pulmonary surfactant (PS) is a surface-active material that lines the air/alveolar fluid interface in mammalian lungs. It plays an important role in vital physiological processes, such as respiratory movement. Its main function is to reduce surface tension at the interface, preventing alveolar collapses at the end-expired state and minimizing the work of breathing (1). This function is achieved by the formation of a surface-active film that consists of lipid monolayers highly enriched in dipalmitoylphosphatidylcholine (DPPC), and bilayer or multilayer structures (surface-associated reservoirs) closely attached to surface monolayers. These layered structures below the surface monolayer were recently confirmed in vitro by fluorescence microscopy (FM) and atomic force microscopy (AFM) (2–5), and also in vivo by electron microscopy (6).

PS is composed of lipids (~90 wt %) and proteins (~10 wt %). The lipids consist mainly of phosphatidylcholines (especially DPPC, ~50 wt %) and smaller but significant amounts of phosphatidylglycerol (PG) and palmitic acid (PA) (7–9). With respect to the proteins, the hydrophobic surfactant protein B (SP-B) has a crucial role in lung functions. SP-B deficiency caused by its gene knockout in mice (10) or by its gene mutation in preterm infants (11,12) can lead to fatal respiratory failure. Moreover, the genetic absence of SP-B induces a deficiency in another hydrophobic surfactant protein, surfactant protein C (SP-C), due to dysfunction of the SP-C proprotein (10). The human SP-B contains 79 amino acids and has a molecular mass of 8.7 kDa (13,14). SP-B has a net charge of +7, which is thought to be essential for electrostatic interactions between its polar residues and the headgroups of negatively charged phospholipids, such as PG (4,15). Given the importance of SP-B for proper PS activity, synthetic peptides based on the amino acid sequence of SP-B have been designed to clarify the mechanism of lipid-protein interactions around the interface and to develop synthetic surfactant preparations containing artificial peptides, such as KL_4 (16–18) and Hel 13-5 (19–21), for patients with respiratory distress syndrome (RDS). Hel 13-5 (NH_2-KLLKLLLKLWLKLLKLLL-COOH) is a monomeric synthetic peptide based on the N-terminal segment of human SP-B. Its structure and surface activity have been investigated thoroughly both in vitro and in vivo. The secondary

Submitted August 1, 2008, and accepted for publication November 20, 2008.

*Correspondence: wosamu@niu.ac.jp

Editor: Huey W. Huang.

0006-3495/09/02/1415/15 $2.00

doi: 10.1016/j.bpj.2008.11.022

conformation of Hel 13-5 was found to be mainly α-helical (20,22). In vivo experiments showed that the PS preparations containing Hel 13-5 improved lung function and activities in surfactant-deficient rats more than Surfacten (Surfactant TA) (23), which is an analog to Survanta (Ross Laboratories, Columbus, OH). Surfacten is a bovine lung surfactant extract supplemented with DPPC, PA, and tripalmitin, and is commonly administered to RDS infants in Japan (24).

Fluid lipids with less ability to sustain high surface pressures are preferentially ejected from the surface upon compression to enrich the monolayers in rigid phospholipids (mainly DPPC) (25,26). In general, this behavior is known as the ''squeeze-out'' phenomenon. The squeeze-out theory classically assumes an idealized, immiscible interaction between liquid-expanded (LE; unsaturated lipid components) and liquid-condensed (LC; saturated lipid components) monolayers. The phenomenon has a close relation to lung surfactant functions such as the formation of surface-associated reservoirs at the adjacent interface and the hysteresis property of respiratory movement. Moreover, it has strongly affected the design of replacement PS preparations for RDS treatment (27,28). However, it has never been made clear how PS molecules perform such physiological and biophysical functions, although structural evidence of the reservoirs by means of electron microscopy has steadily been confirmed (6). Conventionally, the squeeze-out theory based on the immiscible interaction (or phase separation) has dominated the interpretation of PS experiments. Recent studies have provided new information on the mechanism of the squeeze-out action, with a particular focus on the potential interaction of SP-B with anionic PG (15,29–31). However, the contributions of the specific lipid-protein interaction to the squeeze-out and the stability of surface-associated reservoirs are controversial because of the bulkiness and structural complex of SP-B. and the quite different resolutions between microscopic and spectroscopic techniques.

In this study we focused our attention particularly on the specific interaction between negatively charged phospholipid and Hel 13-5 (SP-B mimicking peptide) with net charges of +5. The aim of this study was to elucidate the effect of the specific interaction on in vitro lung functional indices, such as the monolayer phase behavior and morphology, the hysteresis properties of Langmuir isotherms, and the stability of surface-associated reservoirs. Therefore, we used fully saturated lipid systems to eliminate a factor of the LE-LE (or disordered-disordered) attractive interaction between them (26,32–35). We present the isotherms, Brewster angle microscopy (BAM), FM, and AFM for PS model preparations of dipalmitoylphosphatidylglycerol (DPPG) and DPPC/DPPG (4:1, mol/mol) with and without Hel 13-5 under the physiological condition of pH and ionic strength. Recently, there has been increasing interest in AFM, which yields stimulating information on surface topography and the corresponding phase contrast on a nanometer scale, thereby providing new insights into the interaction and biophysical activity of lipids and model peptides during the breathing cycle. These results are compared with previous data obtained in the same manner for DPPC/Hel 13-5 systems to reveal the preferential interaction of PG or PC headgroups with Hel 13-5 during the successive compression and expansion process (20).

MATERIALS AND METHODS

Materials

Peptide synthesis and purification

An SP-B mimicking peptide, Hel 13-5 (NH_2-KLLKLLLKLWLKLLKLLL COOH), was synthesized by Fmoc (9-fluorenylmethoxycarbonyl) chemistry starting from Fmoc-(Leu or Lys)-PEG-PS (polyethylene glycol-polystyrene)-resin (0.6 g, 0.12 mmol) in monitoring the deprotection of Fmoc group by UV absorbance. The resultant crude peptides were passed through a Sephadex G-25 gel filtration chromatography (25 mm × 130 cm). Then the peptides were purified by a preparative C8 HPLC column (20 mm × 250 mm; Cosmosil, nacalai tesque, Kyoto, Japan) with a gradient system of water-acetonitrile containing 0.1% TFA. The purity was confirmed to be >98% by means of an analytical C18 RP-HPLC column (4.6 mm × 250 mm; Cosmocil). The detailed procedures used for synthesis, purification, and basic analysis of the Hel 13-5 peptides were reported previously (36).

Phospholipids and solvents

L-α-dipalmitoylphosphatidylcholine (DPPC; purity >99%) and L-α-dipalmitoylphosphatidylglycerol (DPPG; purity >99%) were obtained from Avanti Polar Lipids (Alabaster, AL). DPPG was supplied as its sodium salt. 1-Palmitoyl-2-[6-[(7-nitro-2-1,3-benzoxadiazol-4-yl)amino]hexanoyl]-*sn*-glycero-3-phosphocholine (NBD-PC) was also purchased from Avanti Polar Lipids as a fluorescent probe. These lipids were used without further purification or characterization. Chloroform (99.7%) and methanol (99.8%) were used as spreading solvents and were obtained from Cica-Merck (Uvasol, Tokyo, Japan) and nacalai tesque (Kyoto, Japan), respectively. Tris(hydroxymethyl) aminomethane (Tris) and acetic acid (HAc) of guaranteed reagent grade for the preparation of a subsolution were purchased from nacalai tesque. Sodium chloride (nacalai tesque) was roasted at 1023 K for 24 h to remove all surface-active organic impurities. The substrate solution was prepared using thrice-distilled water (surface tension = 71.96 mN m^{-1} at 298.2 K and electrical resistivity = 18 MΩcm).

Methods

Surface pressure-area isotherms

The surface pressure (π) of the monolayers was measured using an automated in-house-made Wilhelmy balance. The surface pressure balance (AG-64; Mettler Toledo, Greifensee, Switzerland) had a resolution of 0.01 mN m^{-1}. The pressure-measuring system was equipped with a filter paper (Whatman 541, periphery = 4 cm, Whatman International, Maidstone, England). The trough was made from Teflon-coated brass (area = 750 cm^2), and Teflon-made barriers (both hydrophobic and lipophobic) were used in this study. The compression process of a typical phospholipid, such as DPPC, can reach surface pressures close to 70 mN m^{-1} without leakage of materials by using hydrophilic barriers. A collapse value of DPPC monolayers is a controversial subject in the literature (37–42). Namely, an entire Teflon-made system is possible to prevent adsorption of materials to barriers and to elucidate quantitative analyses up to monolayer collapse states of phospholipids exactly. In this study, the first kink point on the π-A isotherms at higher surface pressures (>50 mN m^{-1}) is defined as a monolayer collapse (37,38,40,41). The surface potential measurement also supports this behavior. Surface pressure (π)-molecular area (A) isotherms were recorded at 298.2 K within ± 0.1 K. Stock

solutions of DPPC (1.0 mM), DPPG (0.5 mM), and Hel 13-5 (0.1 mM) were prepared in chloroform/methanol (2/1, v/v). The spreading solvents were allowed to evaporate for 15 min before compression. The monolayer was compressed at a speed of <0.11 nm^2 molecule^{-1}min^{-1}. Cyclic compression-expansion isotherms (hysteresis curves) were drawn by tracing compression and expansion processes alternately through five cycles at a rate of ~0.24 nm^2 molecule^{-1}min^{-1} (or ~90 cm^2 min^{-1}). The standard deviations (SDs) for molecular surface area and surface pressure were ~0.01 nm^2 and ~0.1 mN m^{-1}, respectively. The pH of the subsolution was controlled with 0.02 M Tris buffer and 0.13 M NaCl, and was adjusted to 7.4 with an adequate amount of HAc.

Surface potential-area isotherms

The surface potential (ΔV) was simultaneously recorded with surface pressure where the monolayer was compressed and expanded at the air/water interface. It was monitored by means of an ionizing ^{241}Am electrode at 1–2 mm above the interface while a reference electrode was dipped into the subsolution. The electrometer (Keithley 614 and 6517, Keithley Instruments, Cleveland, OH) was used to measure the surface potential. The SD for the surface potential was 5 mV (19,43,44).

Brewster angle microscopy

The monolayer was directly visualized by means of a Brewster angle microscope (KSV Optrel BAM 300; KSV Instruments, Helsinki, Finland) coupled to a commercially available film balance system (KSV Minitrough, KSV Instruments Ltd., Finland). The application of a 20 mW He-Ne laser emitting *p*-polarized light of 632.8 nm wavelength and a 10× objective lens allowed a lateral resolution of ~2 μm. The angle of the incident beam to the air/water interface was fixed to the Brewster angle (53.1°) at 298.2 K. The reflected beam was recorded with a high-grade charge-coupled device (CCD) camera (EHDkamPro02; EHD Imaging, Demme, Germany) and the BAM images were digitally saved to the computer's hard disk.

Fluorescence microscopy

The film balance system (KSV Minitrough) was mounted onto the stage of the Olympus microscope BX51WI (Tokyo, Japan) equipped with a 100-W mercury lamp (USH-1030L), an objective lens (SLMPlan50×, working distance = 15 mm), and a 3CCD camera with a camera control unit (IKTU51CU; Toshiba, Tokyo, Japan). The *z*-directional focus on the monolayer was adjusted exactly with the use of an automation controller (MAC 5000; Ludl Electronic Products, Hawthorne, NY). FM observations and compression isotherm measurements were carried out simultaneously. A spreading solution of the samples was prepared as a mixed solution doped with 1 mol % of a fluorescence probe (NBD-PC). The excitation (460 nm) and emission (534 nm) wavelengths were selected by a mirror unit (U-MWIBA3). FM micrographs were directly recorded with the hard disk via an online image processor (DVgate Plus; Sony, Tokyo, Japan) connected to the microscope. Image processing and analysis were carried out with Scion Image Beta 4.02 for Windows software (Scion, Frederick, MD). The total amount of ordered domains (dark contrast regions) was evaluated and expressed as a percentage per frame by dividing the respective frame into dark and bright regions.

Atomic force microscopy

Langmuir-Blodgett (LB) film preparations were carried out with the KSV Minitrough. Freshly cleaved mica (Okenshoji, Tokyo, Japan) was used as a supporting solid substrate for the film deposition (a vertical dipping method). At selected surface pressures, a transfer velocity of 5 mm min^{-1} was used for the film-forming materials on a 0.02 M Tris buffer and 0.13 M NaCl (pH 7.4) at 298.2 K. The transfer occurs such that the hydrophilic part of the monolayer is juxtaposed to the mica while the hydrophobic part is exposed to air. LB films with a deposition rate of ~1 were used in the experiments. The AFM experiments were performed in the air. The LB technique includes the possibility that the original monolayer structures are changed by the electric charge of samples and the physical factor during the deposition procedure. AFM images do not provide completely correct information on the phase behavior at the air/water interface, but can provide helpful information for understanding pulmonary functions. AFM images were obtained using an SPA 400 instrument (SII, Chiba, Japan) at room temperature in the tapping mode, which provided both a topographical image and a phase-contrast image. The tapping-mode images (256 or 512 points per line) were collected with scan rates of 1 Hz using silicon tips (Olympus, Tokyo, Japan) with a nominal spring constant of 1.8 N m^{-1} under normal atmosphere (20,45). The lateral and vertical resolutions were 0.2 and 0.1 nm, respectively. The transferred samples were checked for possible tip-induced deformation by zooming out after a region was scanned.

RESULTS AND DISCUSSION

Isotherm behavior

The surface pressure (π) measured by film balance is commonly used to obtain information on a change in the surface tension (γ) with the surface concentration of the surfactants. The relation between π and γ is given by the equation $\pi = \gamma_0 - \gamma$, where γ_0 represents the surface tension of the subsolution without monolayers. On the other hand, the surface potential (ΔV) provides sensitive information on molecular orientation and conformation normal to the interface depending on the molecular area (A). Thus, coincidence measurements of π-A and ΔV-A isotherms for PS systems contribute to a better understanding of their action and function under compression and expansion. As shown in Fig. 1, typical π-A and ΔV-A isotherms for fully saturated phospholipid systems of DPPG and DPPC/DPPG (4:1, mol/mol), whose ratio is the same as that found in a natural lung lavage (13), were measured to obtain basic information on the phase behavior of monolayers at the air/water interface. The π-A isotherm of pure DPPG monolayers has a kink at ~17 mN m^{-1} ($A = 0.70$ nm^2) corresponding to the first-order transition from the LE to LC state. The collapse pressure of DPPG monolayers is ~56 mN m^{-1} ($A = 0.39$ nm^2), where the transformation of monolayer states (2D) into other states (3D) occurs. The monolayer compressibility, Cs, for each sample was calculated from π-A isotherms using $Cs = (-1/A)(dA/d\pi)$. The inverse compressibility, Cs^{-1}, is expressed against π in the inset of Fig. 1 to distinguish inflection points on π-A isotherms. The transition and collapse pressures indicated by straight-line and dashed arrows, respectively, in Fig. 1 can be determined by analyzing the change in slope of both π-A and ΔV-A isotherms, and the local minimum of Cs^{-1}-π curves (19,45). In the case of the DPPC/DPPG lipid mixture, the transition pressure is ~10 mN m^{-1} ($A = 0.68$ nm^2) and the mixture forms stable monolayers up to ~57 mN m^{-1} ($A = 0.39$ nm^2). In this system, the shape of π-A isotherms is very similar to that for DPPC monolayers reported previously because of the DPPC-enriched contents (20). These π-A isotherms agree well with the data in published studies (25,46,47).

The ΔV values of DPPG show large positive variations from ~0 to ~402 mV upon lateral compression. The sharp jump appears on the ΔV-A isotherm at ~1.25 nm^2, which

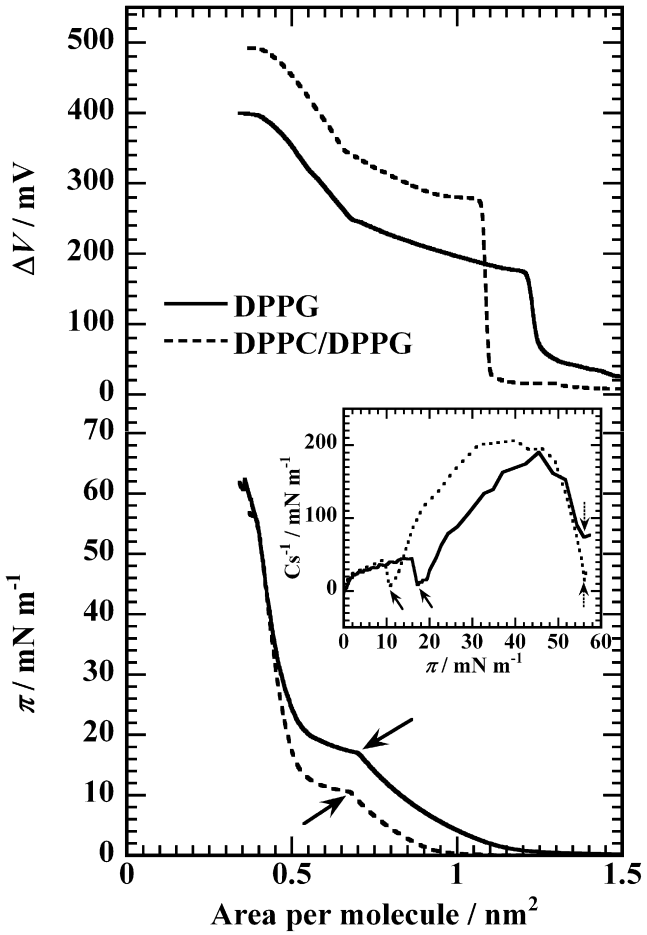

FIGURE 1 Surface pressure (π)-molecular area (A) and surface potential (ΔV)-A isotherms of pure DPPG and DPPC/DPPG (4:1, mol/mol) monolayers under compression in a 0.02 M Tris buffer solution (pH 7.4) with 0.13 M NaCl at 298.2 K. Their inverse compressibility, Cs^{-1}, against π is inserted. The LE/LC transition and monolayer collapse pressures are indicated by straight-line arrows and dashed arrows, respectively.

corresponds to the transition from gaseous phases to LE phases. On further compression after the jump, the ΔV values reach the maximum value (~402 mV) via phase changes from the LE phase through the LC phase to solid state. The increase in ΔV value means an orientational improvement of monolayers, and the close-packed monolayers induced by compression generate the maximum ΔV value with a subsequent plateau, which is characterized by collapsed monolayers or a 3D solid state. The DPPC/DPPG system exhibits a ΔV-A isotherm similar to that of DPPG alone. However, DPPC/DPPG exerts the larger ΔV values (~495 mV) in the close-packed state. This is explained by the fact that the DPPC/DPPG mixtures consist mainly of DPPC, whose monolayer has the maximum ΔV value of ~550 mV, as reported previously (20). Taking into account that the surface density of the end-tail CH_3– group in the close-packed state is almost the same among DPPG, DPPC/DPPG, and DPPC monolayers due to the saturated hydrophobic chains, the difference in maximum ΔV values is attributed to differences in the headgroup of phospholipids (48–50).

As reported previously (5,19,20), Hel 13-5 alone has no kink point and is more expanded, indicating that the Hel 13-5 monolayer is in the disordered state over the whole surface pressure. Therefore, Hel 13-5 forms the disordered film up to ~42 mN m^{-1} (~2.0 nm^2), and the extrapolated area of Hel 13-5 is ~2.6 nm^2, reflecting mainly α-helical structures rather than β-sheet and other conformations (5,22). The ΔV values of Hel 13-5 monotonically increase to ~380 mV under compression, meaning that there is an increase in its surface concentration with no orientational change on lateral compression.

The isotherms for DPPG and DPPC/DPPG (4:1, mol/mol) preparations containing various molar amounts of Hel 13-5 peptides ($X_{\text{Hel 13-5}}$) were examined to elucidate a variation of fundamental properties by the addition of Hel 13-5 at the air/water interface, and the representative data are shown in Fig. 2, A and B, respectively. For the DPPG/Hel 13-5 preparations, all of the π-A isotherms (Fig. 2 A) have an LE/LC transition pressure of ~17 mN m^{-1}, as indicated by a straight-line arrow. The pressure values of the transition are almost the same as ~17 mN m^{-1} in the range of $0 \leq X_{\text{Hel 13-5}} \leq 0.1$. On the other hand, the π-A isotherms for DPPC/DPPG/Hel 13-5 indicate a smaller transition value of ~10 mN m^{-1} over the molar range ($X_{\text{Hel 13-5}}$) from 0 to 0.05, and a slight increase in the value (~13 mN m^{-1}) is observed for monolayers of $X_{\text{Hel 13-5}} = 0.1$. The above results indicate that the interaction between the lipids and Hel 13-5 is very weak at low surface pressures, similar to results obtained in previous systems (5,19,20). At higher surface pressures, both of the π-A isotherms at $X_{\text{Hel 13-5}} = 0.1$ have a plateau (indicated by *dashed arrows*) where Hel 13-5 starts to be gradually squeezed out of the monolayers. There is an obvious difference in the squeeze-out pressure between both the monolayers of $X_{\text{Hel 13-5}} = 0.1$; ~50 mN m^{-1} for DPPG/Hel 13-5 and ~42 mN m^{-1} for DPPC/DPPG/Hel 13-5. Considering the previous results from the PS preparations without abundant PG components, the squeeze-out pressure on π-A isotherms indicates a constant value of ~42 mN m^{-1} corresponding to the collapse pressure of single Hel 13-5 monolayers regardless of compositions and components (5,19,20). As shown in Fig. 3, however, the binary preparations enriched in DPPG show a variation of the squeeze-out pressures (range: 39–49 mN m^{-1}) against $X_{\text{Hel 13-5}}$, whereas the pressures are kept almost constant for DPPC/Hel 13-5 and DPPC/DPPG/Hel 13-5 with a maximum deviation of 5 mN m^{-1}. The variation demonstrates that cationic Hel 13-5 electrostatically interacts with anionic DPPG at high surface pressures, similarly to miscible behavior between normal lipid monolayers (45,51–53); that is, the positive change in pressure at $X_{\text{Hel 13-5}} = 0.1$ suggests that the mutual electrostatic attractive force prevents Hel 13-5 from being squeezed out of DPPG/Hel 13-5 monolayers.

At surface pressures below the plateau, the ΔV-A isotherms for both preparations (Fig. 2, A and B) shift to

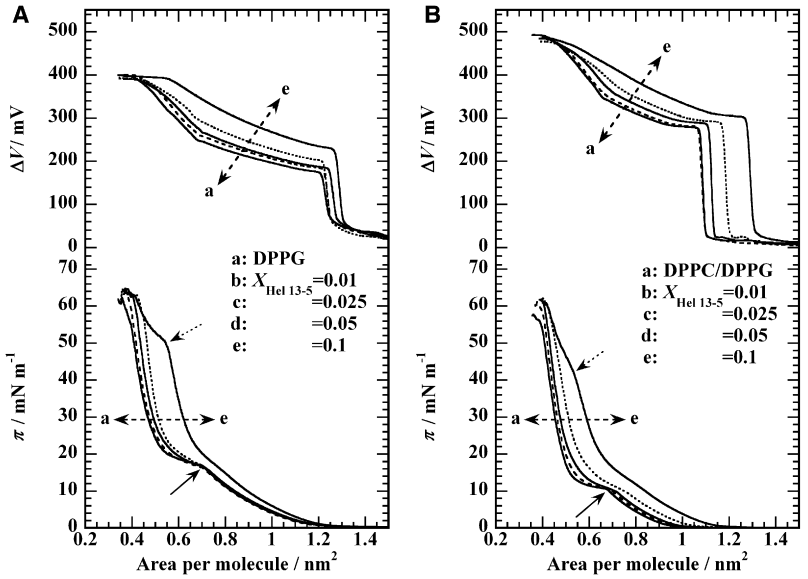

FIGURE 2 Representative compression π-A and ΔV-A isotherms of (A) binary DPPG/Hel 13-5 and (B) ternary DPPC/DPPG (4:1, mol/mol)/Hel 13-5 preparations in a 0.02 M Tris buffer solution (pH 7.4) with 0.13 M NaCl at 298.2 K. The isotherms are displayed as a function of Hel 13-5; $X_{\text{Hel 13-5}} = 0$, 0.01, 0.025, 0.05, and 0.1. The typical LE/LC transition pressures are indicated by straight-line arrows. The onset of a plateau corresponding to the squeeze-out motion of Hel 13-5 is indicated by dashed arrows.

larger ΔV values with increasing Hel 13-5 content. This is attributed to a monotonous increase in ΔV value for a single Hel 13-5 monolayer on compression (5,19,20). On further compression beyond the plateau on π-A isotherms, however, ΔV-A isotherms finally converge to similar ΔV values of ~402 (for DPPG/Hel 13-5) or ~495 mV (for DPPC/DPPG/Hel 13-5), corresponding to the maximum values of the respective lipids without Hel 13-5. This suggests that in the high surface pressure region above the plateau, large proportions of Hel 13-5 are squeezed out and the close-packed monolayers composed mainly of lipid components are formed at the surface.

In situ BAM observations

FM requires a small addition of a fluorescent probe to target monolayers. The probe molecules behave like an impurity and thus may affect the film morphology and phase transitions. On the other hand, BAM, which needs no fluorescent probe and is sensitive to the surface density and anisotropy of phase domains in a monolayer, can be used to avoid this drawback and to confirm the data obtained from FM (45,54). The in situ direct observation of monolayers with BAM has an advantage in analyzing the correct (or original) phase behavior upon lateral compression, although the practical resolution and magnification achieved with BAM are much less compared to those achieved with FM for our system. BAM images represent differences in the local refractive index at the interface due to variations in monolayer density, orientation, and structure. The representative BAM images for the DPPG/Hel 13-5 systems at selected surface pressures are shown in Fig. 4. For pure DPPG monolayers, homogeneous dark images (Fig. S1 in the Supporting Material) are observed below the transition pressure of ~17 mN m^{-1}. Small circular LC domains of DPPG emerge at ~17 mN m^{-1} and grow in size by further compression above the transition pressure (Fig. 4, *left row*). Consequently, the images become homogeneously bright (Fig. S1), corresponding to LC (or solid) phases. The BAM images for pure DPPG monolayers at elevated surface pressures are similar to those reported previously (47). When a small amount of Hel 13-5 is added to DPPG monolayers, the LC domains become quite small in size and dispersed. In the case of the DPPC/DPPG/Hel 13-5 preparations, on the other hand, the effects of the Hel 13-5 addition on the phase behavior of the DPPC/DPPG monolayer can be visualized (Fig. 5). Compared to the BAM images of DPPG alone, the DPPC/DPPG lipid mixture forms larger LC domains with some branches such as a dendrimer (see Figs. 4 and 5) and shows similar phase behavior and growth, i.e., the LC domains shrink in size, keeping the similar domain

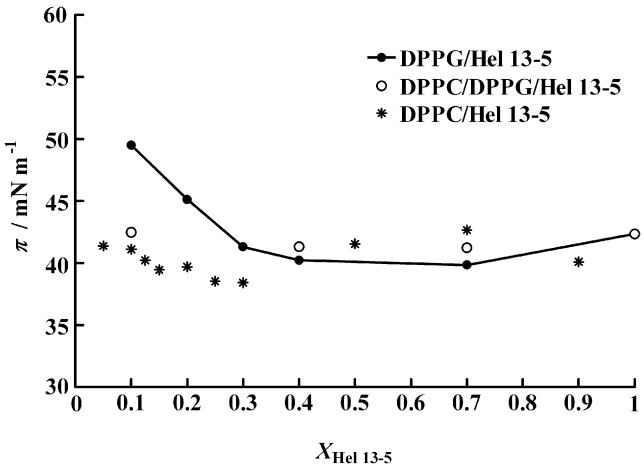

FIGURE 3 Surface pressures of the onset of the plateau against a molar amount of Hel 13-5 ($X_{\text{Hel 13-5}}$) for DPPG/Hel 13-5, DPPC/DPPG (4:1, mol/mol)/Hel 13-5, and DPPC/Hel 13-5. The plots indicate the surface pressure values of means $\pm$ SD; the maximum SD is 0.2 mN m^{-1} for $X_{\text{Hel 13-5}} = 0.7$ (DPPG/Hel 13-5). Note that the error bars are included within the markers. The data for DPPC/Hel 13-5 were obtained from a previous study (20).

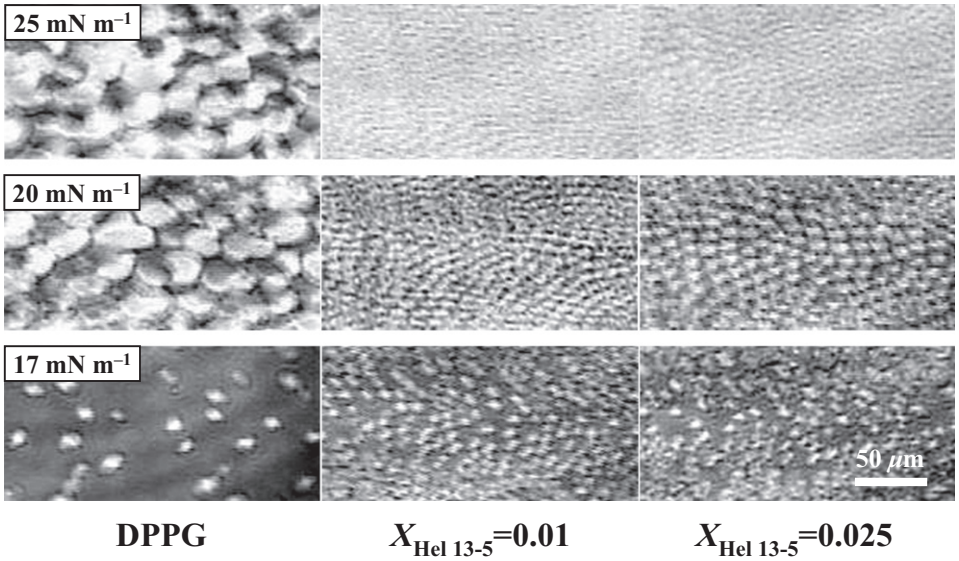

FIGURE 4 Characteristic BAM images of the binary DPPG/Hel 13-5 preparations at $X_{\text{Hel 13-5}} = 0$ (DPPG), 0.01, and 0.025 at selected surface pressures in a 0.02 M Tris buffer solution (pH 7.4) with 0.13 M NaCl at 298.2 K. The scale bar in the lower-right corner represents 50 μm.

shape as Hel 13-5 content increases. The BAM images for DPPC/DPPG/Hel 13-5 indicate that the electrostatic interaction between DPPG and Hel 13-5 is negligible for the domain shape as well as the nucleation process of the LC domains at low surface pressures, due to lower surface concentrations of DPPG compared to the binary system (Fig. 4).

In situ FM observations

Surface textures observed by FM during lipid phase transitions of the model PS systems demonstrate the good performance of surface characteristics. The LE/LC transition can be analyzed by screening the distribution of fluorescent probes in lipid monolayers. The contrast of FM images depends on the difference in solubility of the probes between LE (disordered) and LC (ordered) phases. As a result, the probe molecules are selectively dissolved in LE phases. As mentioned above, there remains the possibility that the probes will affect the original phase behavior of the monolayers. However, the presence of 1 mol % NBD-PC as a fluorescent dye has no influence on the original π-A and ΔV-A isotherms or the domain shapes in BAM images. Shown in Fig. 6 are the selected FM micrographs of the DPPG/Hel 13-5 preparations. For pure DPPG monolayers, the phase behavior and domain shape are quite similar to those obtained from BAM. With increasing surface pressure from 17 to 25 mN m^{-1} (Fig. 6, *left column*), the ratio of LC (dark) domains per image increases from 27% to 78%, which indicates the drastic transformation to LC phases. On further compression beyond 35 mN m^{-1}, the proportion is kept constant at ~100% up to the monolayer collapse (data not shown). The resultant phase behavior and domain shape of pure DPPG monolayers are similar to those reported previously (31). FM images of Hel 13-5 alone are homogeneously bright over the whole surface pressures applied, corresponding to its π-A behavior (5,20).

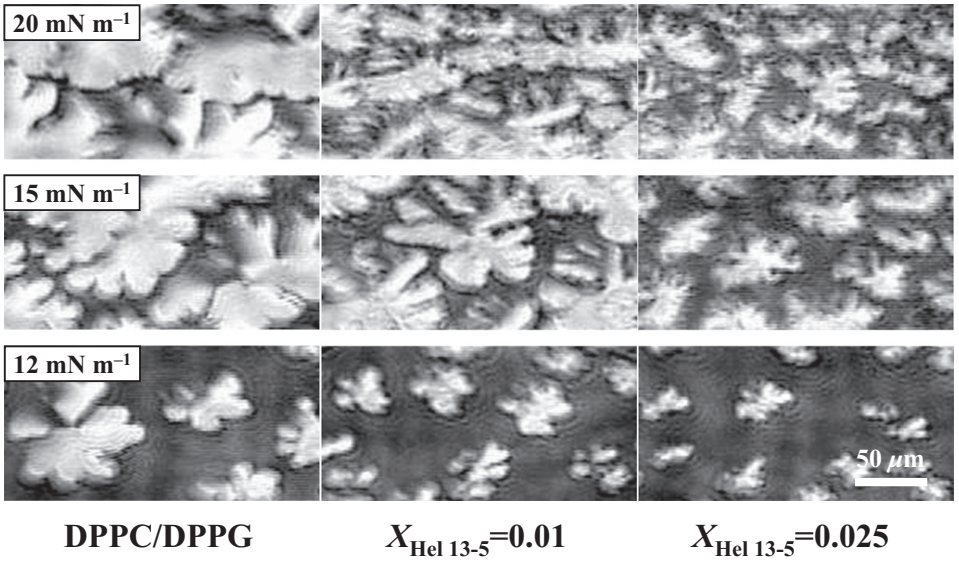

FIGURE 5 Characteristic BAM images of the ternary DPPC/DPPG (4:1, mol/mol)/Hel 13-5 preparations at $X_{\text{Hel 13-5}} = 0$ (DPPC/DPPG), 0.01, and 0.025 at selected surface pressures in a 0.02 M Tris buffer solution (pH 7.4) with 0.13 M NaCl at 298.2 K. The scale bar in the lower-right corner represents 50 μm.

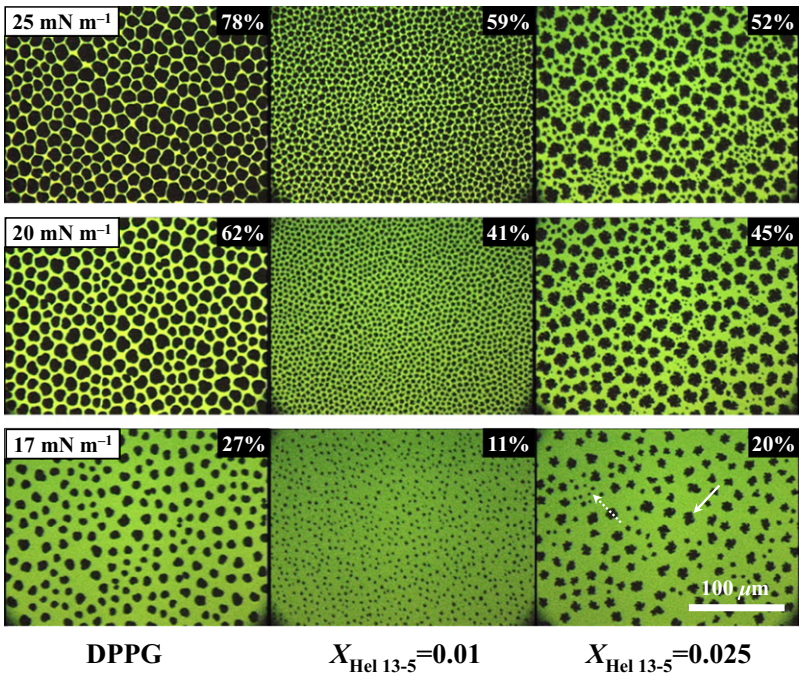

FIGURE 6 Representative FM images of the binary DPPG/Hel 13-5 preparations at $X_{\text{Hel 13-5}} = 0$ (DPPG), 0.01, and 0.025 at selected surface pressures in a 0.02 M Tris buffer solution (pH 7.4) with 0.13 M NaCl at 298.2 K. Percentages (%) refer to the ratio of ordered domains in the micrograph. The monolayers contain 1 mol % fluorescent probe (NBD-PC). The scale bar in the lower-right corner represents 100 μm.

As for the phase behavior of the DPPG/Hel 13-5 preparations, unique trends are observed by the systematical FM examination, which cannot be found by BAM for our system. Unfortunately, this is due to the lower magnification and resolution of the BAM apparatus compared to the FM one. Over the range of $0 < X_{\text{Hel 13-5}} \leq 0.01$, the LC domains of DPPG gradually and monotonously shrink in size with increasing $X_{\text{Hel 13-5}}$, as seen from the reduction in LC percentages. This shows that at low and middle surface pressures, the electrostatic interaction between the two molecules is very weak for the change in the phase behavior, nucleation process, and domain shape due to low surface concentrations of Hel 13-5. In the $0.01 < X_{\text{Hel 13-5}} \leq 0.05$ range, FM images show two kinds of nonfluorescent domains (indicated by *straight-line* and *dashed arrows* in Fig. 6) at $X_{\text{Hel 13-5}} = 0.025$ (17 mN m^{-1}). When the molar fractions of Hel 13-5 decrease from 0.025, the two populations are observed up to $X_{\text{Hel 13-5}} = 0.013$, as seen in Fig. S2; that is, the phase behavior for the DPPG/Hel 13-5 monolayers varies on the border of $X_{\text{Hel 13-5}} = 0.01$. The smaller domains indicated by the dashed arrow are not intermediate to the larger ones, and the two domains above grow independently in size and number with an increase in surface pressure. As Hel 13-5 contents increase from $X_{\text{Hel 13-5}} = 0.025$ to 0.05, the ratio of the larger domains reduces and the smaller domains come to dominate the images (data not shown). Assuming no mutual interaction, the percentage of LC domains should be expected to monotonously decrease with increasing $X_{\text{Hel 13-5}}$. However, the percentages between $X_{\text{Hel 13-5}} = 0.01$ and 0.025 remain almost the same. This irregular behavior implies the existence of a specific interaction between DPPG and Hel 13-5 such as a a miscible monolayer. For the FM images of $X_{\text{Hel 13-5}} = 0.01$ and 0.025 at 17 mN m^{-1}, the percentages are apparently rather different. However, they regularly increase as the Hel 13-5 contents increase from $X_{\text{Hel 13-5}} = 0.01$ to 0.025 (Fig. S2). Thus, the smaller and larger domains may consist of free DPPG molecules and DPPG/Hel 13-5 complexes, respectively. There is a possibility that the phase behavior observed here results from just a delayed nucleation. If the smaller domains are characterized by a delayed nucleation, the domains should approach to the larger domains indicated by the straight-line arrow (Fig. 6) with increasing time. However, the smaller domains remain in the images for up to 180 min (Fig. S3). Moreover, the smaller domains do not vary in size and number to a large extent for $X_{\text{Hel 13-5}} = 0.025$ (the DPPG/Hel 13-5 system) regardless of a further increase in surface pressure (Fig. S4). Thus, it is unlikely that the two populations can be attributed to the delayed nucleation in this system. At $X_{\text{Hel 13-5}} \geq 0.1$, the homogeneously bright images of disordered phases appear in FM for our system regardless of surface pressures.

Representative FM images of the DPPC/DPPG/Hel 13-5 preparations are shown in Fig. 7. For the DPPC/DPPG (4:1, mol/mol) lipid mixture, the FM images show phase behavior similar to that obtained by BAM. The domain shape is different from that of pure DPPG and DPPC (31), which indicates that DPPC and DPPG form a miscible monolayer. With increasing Hel 13-5 content, anticlockwise LC domains of the lipid mixture shrink in size, and correspondingly the ratio of LC domains gradually decreases at 20 mN m^{-1}. The irregular increase in the percentage at lower surface pressures of 12 and 15 mN m^{-1} is attributed to a slight depression (<0.6 mN m^{-1} in $0 \leq X_{\text{Hel 13-5}} \leq 0.05$) of LE/LC transition pressures by the Hel 13-5 addition. Here, the resultant FM images do not show the specific

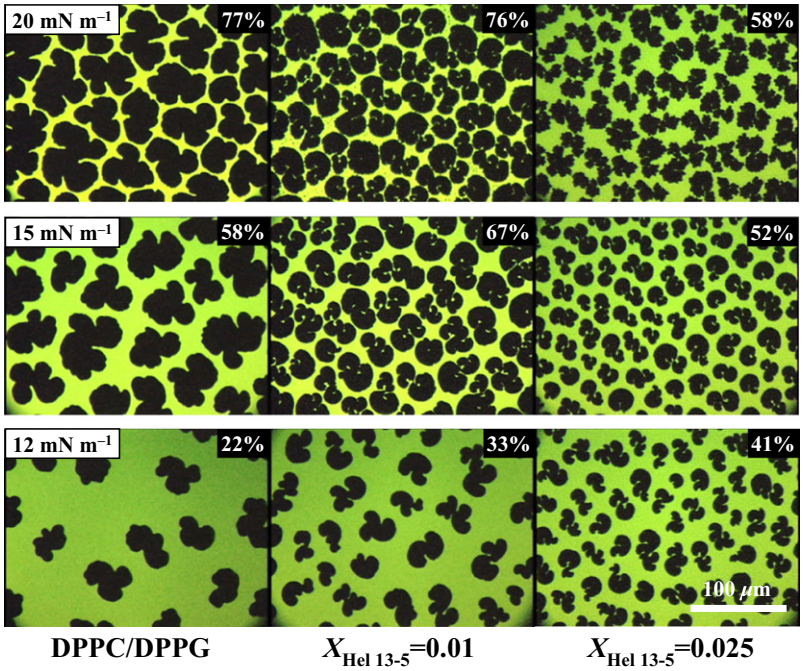

FIGURE 7 Representative FM images of the ternary DPPC/DPPG (4:1, mol/mol)/Hel 13-5 preparations at $X_{\text{Hel 13-5}} = 0$ (DPPC/DPPG), 0.01, and 0.025 at selected surface pressures in a 0.02 M Tris buffer solution (pH 7.4) with 0.13 M NaCl at 298.2 K. Percentages (%) refer to the ratio of ordered domains in the micrograph. The monolayers contain 1 mol % fluorescent probe (NBD-PC). The scale bar in the lower-right corner represents 100 μm.

behavior that is observed in the binary DPPG/Hel 13-5 preparations. This behavior would result from the fact that the ratio of DPPG to Hel 13-5 is too small and/or that the miscible interaction between DPPC and DPPG predominates over the electrostatic interaction between DPPG and Hel 13-5. At $\pi \geq 20$ mN m^{-1}, the LC domains become irregular in edge and confused. The change supports the latter aspect for a balance of the two interactions; that is, with increasing surface pressure, the electrostatic interaction becomes stronger and stronger due to the shortened intermolecular distance between DPPG and Hel 13-5, and thus DPPG can interact with DPPC as well as Hel 13-5.

We previously proposed a ''refluorescence'' phenomenon for FM observation of PS models, which provides what we believe is novel morphological evidence of squeeze-out events in Hel 13-5 (5,19). When pulmonary preparations containing fluid lipids, such as anionic PG and dissociated palmitic acid (PA), are observed by FM, the FM contrast clearly varies before and after the squeeze-out of Hel 13-5 due to the recovery from concentration quenching of FM probes. At the stage of the squeeze-out event, Hel 13-5 is ejected together with fluid components, including FM probes, and consequently the surface concentration of FM probes decreases to visualize the LE/LC coexistence again. In the preparations used in this study, however, there is no variation in contrast corresponding to the squeeze-out action, which means that major parts of saturated DPPC and DPPG are not eliminated from the surface, despite the squeeze-out of Hel 13-5.

Hysteresis behavior

During exhalation, fluid components in PSs are ejected from the air/water interface to be stored in surface-associated reservoirs or 3D aggregates, preventing the alveolar collapse. Under inhalation, on the other hand, the squeezed-out molecules reenter with a delay and then spread back into monolayers. This process is commonly called respreading. The squeeze-out motion and respreading of the fluid components generate a large hysteresis loop in typical pressure-volume curves for lungs. Repeated compression-expansion isotherm measurements on a trough allow us to assess such biophysical functions in vitro for pulmonary preparations. In particular, both the large hysteresis area and reproducible hysteresis loops are very important for pulmonary function and activity (55). To elucidate the squeeze-out motion across the interface, a certain degree of the plateau region is desired on π-A isotherms (55–57). Therefore, we focus on the preparations of $X_{\text{Hel 13-5}} = 0.1$ in both the systems investigated above, which contain the minimum amount of Hel 13-5. In addition, the data obtained here were compared with those for the previous preparation of DPPC/Hel 13-5 ($X_{\text{Hel 13-5}} = 0.1$) (20). Repeated cycling π-A and ΔV-A isotherms of the preparations from the first to the fifth rounds were measured. These monolayers were compressed up to the respective collapse pressure and then expanded to the starting molecular areas. This process was successively repeated to elucidate the reproducibility of the respreading process within a monolayer. For pure DPPG (Fig. 8 *A*), both π-A and ΔV-A isotherms indicate a good reproducibility from the first to the fifth cycles and a slight hysteresis loop, as expected. This means that the variational modes of molecular packing, surface concentration, and orientation of monolayers depend simply on the molecular area regardless of the difference in stage through the compression-expansion cycle. On the other hand, the DPPG/Hel 13-5 preparation ($X_{\text{Hel 13-5}} = 0.1$) exhibits large

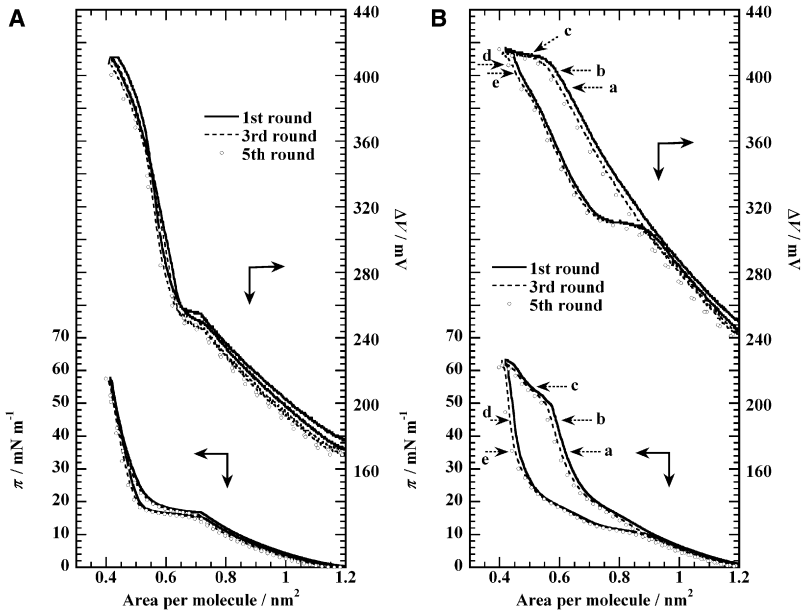

FIGURE 8 Cyclic compression and expansion isotherms of (*A*) pure DPPG and (*B*) the DPPG/Hel 13-5 preparation at $X_{\text{Hel 13-5}} = 0.1$ on a 0.02 M Tris buffer solution (pH 7.4) with 0.13 M NaCl at 298.2 K. The compression-expansion cycle was performed five times at a compression rate of ~90 $\text{cm}^2\ \text{min}^{-1}$. Typical stages on hysteresis curves in *B* are indicated by dashed arrows; (*a*) 35 mN m^{-1}, (*b*) 45 mN m^{-1}, and (*c*) 55 mN m^{-1} during the compression process; and (*d*) 45 mN m^{-1} and (*e*) 35 mN m^{-1} during the expansion process.

hysteresis loops on both π-*A* and ΔV-*A* isotherms (Fig. 8 *B*). As mentioned above, the π-*A* hysteresis curves have a plateau at high surface pressures (~50 mN m^{-1}) during lateral compression, where the squeeze-out action and the subsequent formation of 3D aggregates adjacent to the interface gradually occur. In addition, the collapse pressure is enhanced compared to that of pure DPPG. This can be attributed to the stabilization of surface monolayers by the ejected Hel 13-5 (5,19,20). In this case particularly, the electrostatic interaction between the DPPG headgroup and the polarized moiety of squeezed-out Hel 13-5 contributes to the stability. Under expansion, the squeezed-out Hel 13-5 molecules reenter the interface from the aggregates at the slower speed relative to the expansion rate of movable barriers, resulting in a rapid reduction of surface concentrations or surface pressures (58). Thus, large hysteresis is generated on the cyclic π-*A* isotherms. It is also notable that the ΔV-*A* isotherms for the DPPG/Hel 13-5 preparation show large hysteresis loops. As far as we know, hysteresis for cyclic ΔV-*A* isotherms has never been reported, although a few articles on ΔV-*A* isotherms for pulmonary preparations during repeated compression and expansion have been published (5,19,59). In this study, we detected for the first time, to our knowledge, large hysteresis on the cyclic ΔV-*A* isotherms for the DPPG/Hel 13-5 preparation. During compression, the ΔV-*A* isotherms have a plateau corresponding to that on the π–*A* isotherms (the region indicated by *dashed arrow c* in Fig. 8 *B*). According to the conventional aspect, the plateau on the ΔV-*A* isotherms means that the squeeze-out phenomenon of Hel 13-5 progresses mainly with same orientation of DPPG monolayers retained. However, the interpretation itself cannot explain why the hysteresis loop of ΔV-*A* isotherms is produced especially for the DPPG/Hel 13-5 among the many kinds of PS preparations (5,19,20,23,59). Judging from the morphological phase behavior with FM observations ($X_{\text{Hel 13-5}} = 0.025$; Fig. 6), the interfacial behavior of Hel 13-5 in the squeeze-out region during compression can be divided into the following two processes: 1), close packing as a monolayer with DPPG at the interface; and 2), squeezing-out into the subsolution. Although these two processes can be easily expected, they are completely and evidently separated, which is caused by the electrostatic interaction particularly in the binary system. In the plateau region under compression, Hel 13-5 is preferentially eliminated into the subsolution, with the molecular orientation of surface monolayers kept almost constant, and the specific interaction stabilizes both the squeezed-out Hel 13-5 beneath the monolayers and the mixed monolayers with Hel 13-5 at the interface. During expansion, the resultant packed monolayers above respread and then the molecular ordering and orientation are released again along the expansion of molecular area in the region of $0.40\ \text{nm}^2 < A \leq 0.70\ \text{nm}^2$. In the subsequent plateau ($0.70\ \text{nm}^2 < A \leq 0.85\ \text{nm}^2$), the squeezed-out Hel 13-5 molecules stepwise reenter the surface due to the low surface concentration of the monolayers. This independent action is supported by the following facts: the inclination of ΔV-*A* isotherms ($0.40\ \text{nm}^2 < A \leq 0.70\ \text{nm}^2$) and the plateau ($0.70\ \text{nm}^2 < A \leq 0.85\ \text{nm}^2$) in the expansion process are considerably similar to those observed during compression at $0.55\ \text{nm}^2 < A \leq 0.85\ \text{nm}^2$ and $0.40\ \text{nm}^2 < A \leq 0.55\ \text{nm}^2$, respectively. These mechanisms can explain why the large hysteresis is produced in the cyclic ΔV-*A* isotherms.

For the DPPC/DPPG mixture without Hel 13-5 (Fig. 9 *A*), both cyclic π-*A* and ΔV-*A* isotherms indicate similar behavior to pure DPPG (Fig. 8 *A*). In contrast, the addition of Hel 13-5 ($X_{\text{Hel 13-5}} = 0.1$) produces a hysteresis on both π-*A* and ΔV-*A* isotherms for the DPPC/DPPG/Hel 13-5

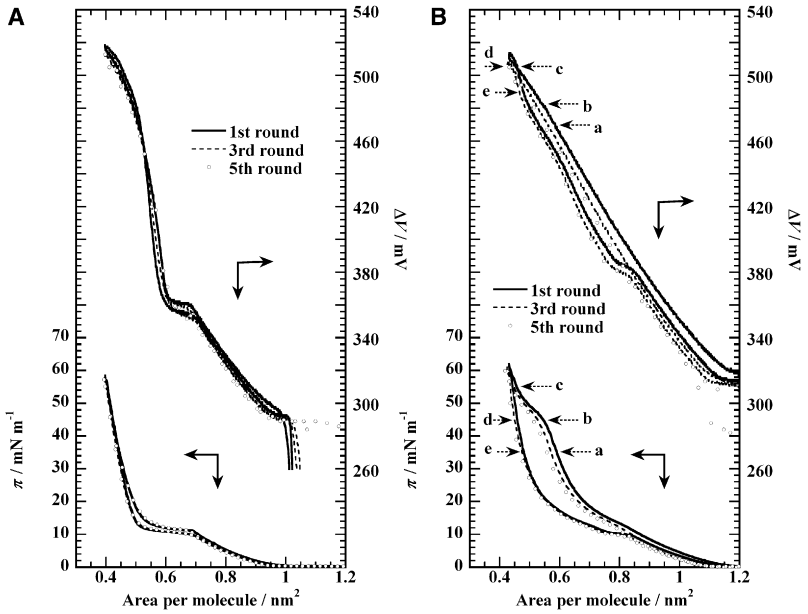

FIGURE 9 Cyclic compression and expansion isotherms of (*A*) DPPC/DPPG (4:1, mol/mol) and (*B*) the DPPC/DPPG (4:1, mol/mol)/Hel 13-5 preparation at $X_{\text{Hel 13-5}} = 0.1$ in a 0.02 M Tris buffer solution (pH 7.4) with 0.13 M NaCl at 298.2 K. The compression-expansion cycle was performed five times at a compression rate of ~90 $\text{cm}^2\ \text{min}^{-1}$. Typical stages on hysteresis curves in *B* are indicated by dashed arrows; (*a*) 35 mN m^{-1}, (*b*) 45 mN m^{-1}, and (*c*) 55 mN m^{-1} during the compression process; and (*d*) 45 mN m^{-1} and (*e*) 35 mN m^{-1} during the expansion process.

preparation (Fig. 9 *B*), just like the DPPG/Hel 13-5 system. However, the hysteresis on both π-*A* and ΔV-*A* isotherms is smaller in loop size than those of the binary mixture in Fig. 8 *B*. In particular, the plateau on the ΔV-*A* isotherms under compression is unclear or disappears. Furthermore, the DPPC/Hel 13-5 preparation at $X_{\text{Hel 13-5}} = 0.1$ showed the hysteresis on π-*A* isotherms, not on ΔV-*A* isotherms (data not shown) (20). Although the preparations had the same Hel 13-5 contents, a depression in the proportion of DPPG was found to reduce hysteresis properties on π-*A* and especially on ΔV-*A* isotherms, which suggests that an appearance of the clear plateau and hysteresis on cyclic ΔV-*A* isotherms indicates a specific interaction between DPPG and Hel 13-5. This interaction contributes deeply to pulmonary functions such as regulation of the squeeze-out event, 3D aggregates, and orientation of surface monolayers. As for the DPPC/Hel 13-5 system with no mutual electrostatic interactions (20), both of the above-mentioned processes for Hel 13-5 were simultaneously carried out during compression and expansion. Judging from these hysteresis data, it is very possible that PG groups in PS play a crucial role in the stabilization of surface-associated reservoirs and the orientational control of surface monolayers by electrostatic interaction with cationic SP-B.

AFM observations

Lipid/peptide films were deposited onto mica, and the topography and the corresponding phase contrast image were subsequently visualized by AFM in tapping mode to investigate the effect of the squeeze-out motion on phase behavior under compression and to understand respreading of the ejected Hel 13-5 under expansion. Here the systems of DPPG, DPPC/DPPG (4:1, mol/mol), and DPPC containing Hel 13-5 of $X_{\text{Hel 13-5}} = 0.1$ were examined as an LB film. The hysteresis isotherm for the DPPC/Hel 13-5 ($X_{\text{Hel 13-5}} = 0.1$) monolayer was previously reported (20). The LB films were fabricated at the desired surface pressures indicated by dashed arrows (*a*–*e*) in Figs.8 *B* and 9 *B*. The DPPC/Hel 13-5 films were deposited at the corresponding surface pressures in the same manner. To investigate the phase behavior of $X_{\text{Hel 13-5}} = 0.1$, whose ordered domains were not detected by either BAM or FM, we obtained AFM measurements for the systems. For the DPPG/Hel 13-5 preparation (Fig. 10, *left column*), the AFM height image at 35 mN m^{-1}, where the squeeze-out has not yet occurred, shows two different phases. Considering the diameter of α-helical Hel 13-5 (~1.0 nm) and the height of nontilted phospholipids with saturated dipalmitoyl chains (~2.5 nm) (20), bright networks and dark domains represent DPPG and Hel 13-5 monolayers, respectively. The corresponding phase-contrast image also exhibits the two phases in an inverse contrast (data not shown). The height difference between the two (0.9 ± 0.2 nm) agrees well with the theoretical one (see Table 1). Upon compression of the monolayer, protrusion masses are formed at 45 mN m^{-1}, appearing as bright discs. The protrusions exist on DPPG monolayers and the difference is 3.3 ± 0.2 nm. According to other AFM studies and previous work (3,20,26,32), the protrusions are made of the ejected Hel 13-5 from surface monolayers on compression. The intermediate state toward the squeeze-out is indicated by arrows in Fig. 10. The regions contain smaller protrusions with a height of 1.2 ± 0.3 nm. Hel 13-5 itself, with a collapse pressure of ~42 mN m^{-1}, has an intermediate state toward monolayer collapse below its collapse pressure (20). Thus, the electrostatic interaction between the two may induce the formation of the intermediate state even below the squeeze-out pressure

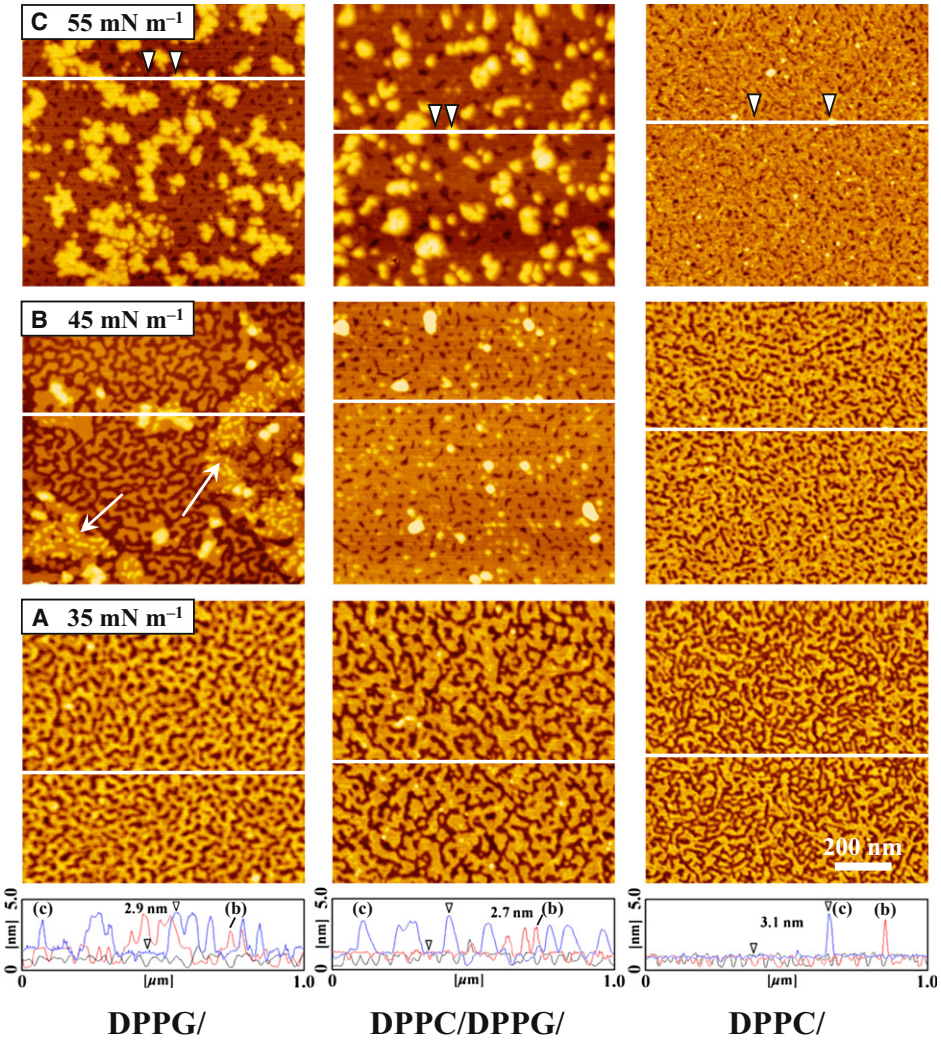

FIGURE 10 Typical AFM topographic images of DPPG/Hel 13-5, DPPC/DPPG (4:1, mol/mol)/Hel 13-5, and DPPC/Hel 13-5 preparations at $X_{\text{Hel 13-5}} = 0.1$ in a 0.02 M Tris buffer solution (pH 7.4) with 0.13 M NaCl at 298.2 K. The monolayers for DPPG/Hel 13-5 and DPPC/DPPG/Hel 13-5 were transferred onto mica at (*A*) 35, (*B*) 45, and (*C*) 55 mN m^{-1} upon first compression, as indicated by dashed arrows in Figs. 8 *B* and 9 *B*, respectively. For DPPC/Hel 13-5, the films were deposited at the corresponding surface pressures in the same manner. The scan area is 1 × 1 μm and the scale bar in the lower-right corner represents 200 nm. The cross-sectional profiles along the scanning line (*white line*) are given below each column; 35 mN m^{-1} (*black line*); 45 mN m^{-1} (*red line*); 55 mN m^{-1} (*blue line*). The height difference between the arrowheads is indicated in the cross-sectional profile.

(~50 mN m^{-1}). Film topography alters dramatically just when the film is further compressed to 55 mN m^{-1}, where Hel 13-5 has been squeezed out of the interface. In comparison to the AFM images at lower surface pressures, the domains of Hel 13-5 monolayers considerably reduce and the protrusions increase in number and lateral size. The protrusion height (3.1 ± 0.6 nm) is very similar to that at 45 mN m^{-1}, corresponding to two to four layers of a Hel 13-5 molecule. Of interest, some of the protrusions tend to come close together to form a clustered aggregate, like a cloud.

In the case of the DPPC/DPPG/Hel 13-5 preparation (Fig. 10, *middle column*), the AFM image at 35 mN m^{-1} (below the squeeze-out pressure) shows the two different contrasts similarly to that for the DPPG/Hel 13-5 system. When the film is compressed beyond the squeeze-out pressure of ~42 mN m^{-1}, the protrusions are formed on the DPPC/DPPG monolayers (bright regions) and the domains

TABLE 1 Height differences obtained by AFM for DPPG/, DPPC/DPPG/, and DPPC/Hel 13-5 preparations

	Compression						Expansion			
	35 mN/m		45 mN/m		55 mN/m		45 mN/m		35 mN/m	
Surfactant model system at $X_{\text{Hel 13-5}} = 0.1$	A	B	A	B	A	B	A	B	A	B
DPPG/Hel 13-5	0.9	–	1.3	3.3	1.3	3.1	1.4	4.0	1.4	4.2
DPPC/DPPG/Hel 13-5	1.0	–	1.0	3.3	1.1	2.8	0.7	3.0	0.6	1.8
DPPC/Hel 13-5	0.9	–	0.9	1.0	0.6	2.5	0.6	0.9	0.7	1.1

Note that results are expressed as means [nm] with maximum SD 0.8 nm.
A: Height differences between phospholipids and Hel 13-5 within a monolayer.
B: Height differences between phospholipid monolayers and squeezed-out Hel 13-5.

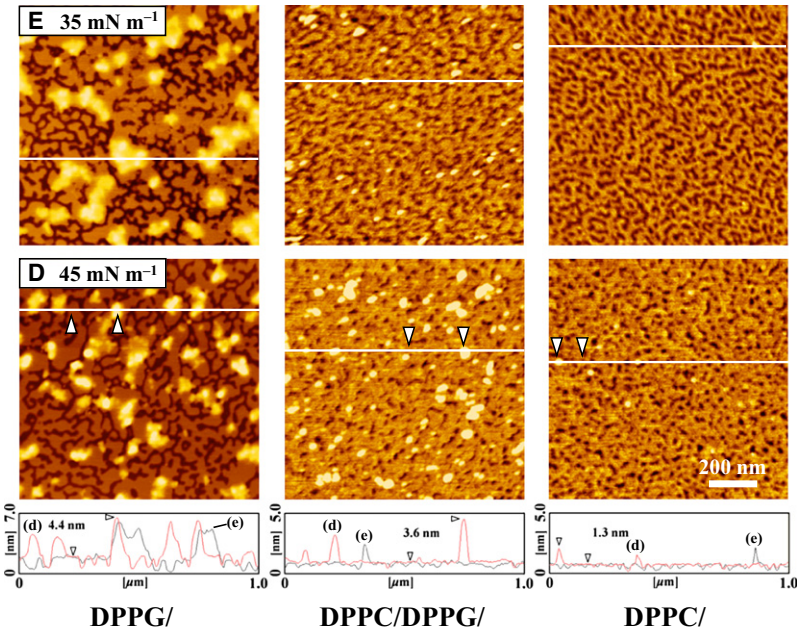

FIGURE 11 Typical AFM topographic images of DPPG/Hel 13-5, DPPC/DPPG (4:1, mol/mol)/Hel 13-5, and DPPC/Hel 13-5 preparations at $X_{\text{Hel 13-5}} = 0.1$ in a 0.02 M Tris buffer solution (pH 7.4) with 0.13 M NaCl at 298.2 K. The monolayers for DPPG/Hel 13-5 and DPPC/DPPG/Hel 13-5 were transferred onto mica at (*D*) 35 and (*E*) 45 mN m^{-1} upon first expansion, as indicated by dashed arrows in Figs.8 *B* and 9 *B*, respectively. For DPPC/Hel 13-5, the films were deposited at the corresponding surface pressures in the same manner. The scan area is 1×1 μm and the scale bar in the lower-right corner represents 200 nm. The cross-sectional profiles along the scanning line (*white line*) are given below each column; 35 mN m^{-1} (*black line*); 45 mN m^{-1} (*red line*). The height difference between the arrowheads is indicated in the cross-sectional profile.

of Hel 13-5 monolayers decrease to a large extent in the LB film of 45 mN m^{-1}. Then, at 55 mN m^{-1} the protrusion masses increase in number and lateral size to form a disc-like particle tens of nanometers in diameter. For the DPPC/Hel 13-5 preparation (Fig. 10, *right column*), phase behavior similar to that of the other systems is also observed before and after the squeeze-out pressure (~42 mN m^{-1}). However, the protrusions observed at 45 and 55 mN m^{-1} differ considerably in shape and number. At 55 mN m^{-1}, in particular, the squeezed-out Hel 13-5 has a tendency to disperse to form a dot-like aggregate.

Judging from the AFM images at 55 mN m^{-1}, the lateral size of the aggregates formed differs among the three preparations described above, although all of them exhibit protrusions with a similar height of ~3.0 nm. In addition, the masses of the ejected Hel 13-5 disperse and become smaller in lateral size with a decrease in DPPG content of the preparations. Given that the preparations shown in Fig. 10 contain the equimolar Hel 13-5 ($X_{\text{Hel 13-5}} = 0.1$), it is strongly suggested that the electrostatic interaction between DPPG and Hel 13-5 plays an important role in the lateral growth and organization of squeezed-out products at high surface pressures. The surface concentration of monolayers with anionic charges may control stabilization of the ejected Hel 13-5.

Shown in Fig. 11 are the AFM height images of the LB films described above for DPPG, DPPC/DPPG (4:1, mol/mol), and DPPC with Hel 13-5 ($X_{\text{Hel 13-5}} = 0.1$) under the first expansion cycle. As for the DPPC/DPPG/Hel 13-5 (*middle column*) and DPPC/Hel 13-5 (*right column*) preparations, the protrusions become smaller in diameter and number, and correspondingly the dark regions of Hel 13-5 monolayers increase with decreasing surface pressure from 45 to 35 mN m^{-1}. In addition, the height of the protrusions becomes <2.0 nm (Table 1). It is notable that the height of protrusions for DPPC/Hel 13-5 approaches ~1.0 nm rapidly at 45 mN m^{-1} under expansion. On the other hand, a gradual reduction in height is observed for DPPC/DPPG/Hel 13-5. These results reveal that the respreading of the squeezed-out Hel 13-5 is improved along the expansion cycle. In the case of the DPPG/Hel 13-5 system (Fig. 11, *left column*), however, there is a clear difference in phase behavior compared to the other mixtures. Despite the decreasing surface pressure (down to 35 mN m^{-1}), the protrusions continue to retain their shape and size laterally and vertically. This means that the ejected Hel 13-5 molecules do not reenter the interface, but are kept below the DPPG monolayer for a while after the films expand. It is demonstrated that the squeezed-out Hel 13-5 is stabilized beneath the interface under expansion by the electrostatic interaction with the surface DPPG monolayers. Accordingly, the surface monolayers are restricted to some extent by the ejected Hel 13-5. This retention of the protrusions strongly supports the notion that the independent emergence of the eliminated Hel 13-5 to the surface takes place after the relaxation of surface monolayers under expansion (Fig. 8 *B*).

As for the DPPG/Hel 13-5 preparation, where Hel 13-5 is surrounded by abundant anionic DPPG, the characteristic behavior induced by the electrostatic interaction is made clear by the results obtained here. Scheme 1 provides a possible explanation for the interaction under film expansion. Considering the saturated acyl chains of DPPG and the results of compression isotherms (Fig. 2), major parts of DPPG would not be ejected together with Hel 13-5, but would remain at the interface as a monolayer during the

squeeze-out process. In previous studies that used pulmonary preparations containing PG with unsaturated chains, the PG components were squeezed out of surface monolayers together with Hel 13-5 (5,19). At low surface pressures, the electrostatic interaction is very weak due to the long intermolecular distance between DPPG and Hel 13-5. The lateral compression of the films reduces the above distance within the monolayer state and the interaction accordingly becomes stronger, resulting in variation of the squeeze-out pressure (Fig. 3). Upon further compression beyond the squeeze-out pressure, Hel 13-5 is preferentially eliminated from the interface and forms mass aggregates like surface-associated reservoirs beneath the surface DPPG monolayers (Scheme 1 *A*). The aggregates are larger in lateral size compared with the other preparations (Fig. 10). Therefore, the electrostatic interaction contributes to the formation and stabilization of the aggregates. During the expansion cycle, the surface monolayers respread to the interface, where the ejected Hel 13-5 is kept beneath the monolayers (Scheme 1 *B*). Then, when the surface concentration of monolayers decreases to a proper extent, the squeezed-out Hel 13-5 molecules reenter the surface (Scheme 1 *C*). The squeezed-out Hel 13-5 is stabilized by the negatively charged headgroup of DPPG monolayers to stay longer beneath the interface, especially in the binary system. Consequently, the specific interaction generates larger hysteresis loops on the cyclic π-*A* and ΔV-*A* isotherms compared to the other preparations as shown in Fig. 8 *B*.

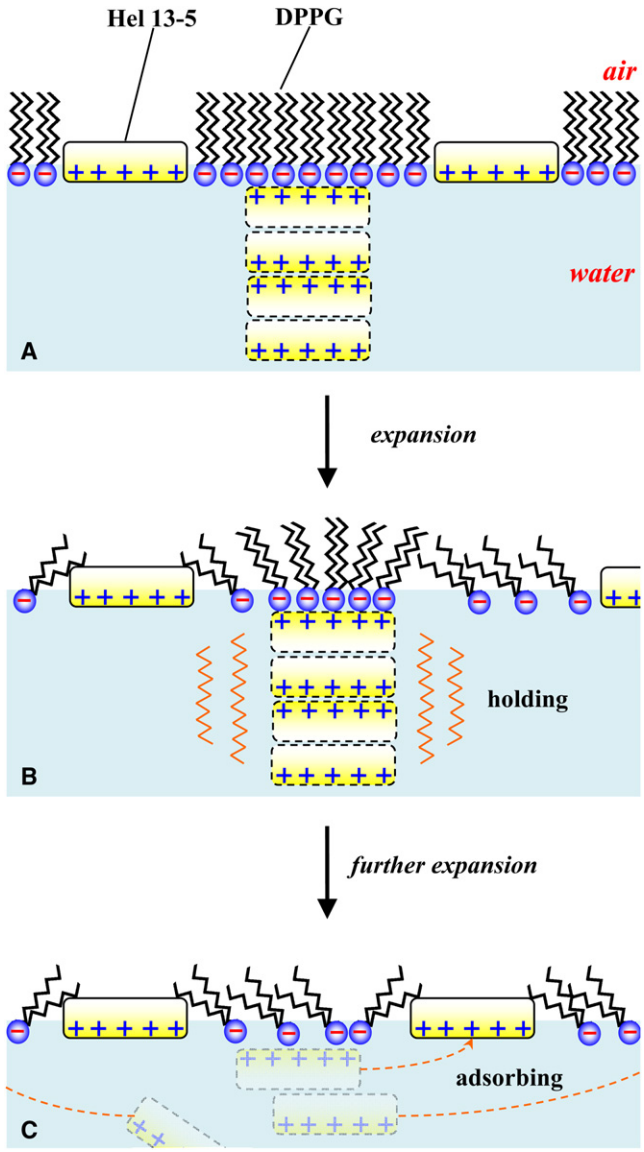

SCHEME 1 Possible explanation for the specific interaction between anionic DPPG and cationic Hel 13-5 in the model pulmonary system of DPPG/Hel 13-5 during expansion. (*A*) the close-packed state before expansion, (*B*) middle surface pressures ($0.40\ nm^2 < A \leq 0.70\ nm^2$ in Fig. 8 *B*), and (*C*) low surface pressures ($0.70\ nm^2 < A \leq 0.85\ nm^2$ in Fig. 8 *B*). Dashed-line rectangles mean squeezed-out Hel 13-5 into the subphase.

CONCLUSIONS

In this work, PS model preparations containing a synthetic peptide (Hel 13-5) were investigated to clarify the importance of the specific interaction between anionic phospholipid of DPPG and cationic Hel 13-5 for pulmonary functions. In particular, fully saturated phospholipid systems were utilized to eliminate the miscibility behavior between phospholipids and Hel 13-5, such as a disordered-disordered attractive interaction, as a factor. At low surface pressures, DPPG/Hel 13-5 monolayers form two kinds of ordered domains with different diameters induced by the mutual electrostatic interaction, and then the domains grow independently upon compression in FM images. In the DPPC/DPPG/Hel 13-5 preparation, the electrostatic interaction, which competes with the miscible interaction between DPPC and DPPG within a monolayer, becomes larger upon compression due to the shorter distance between DPPG and Hel 13-5 molecules. In addition, the existence of the interaction is supported by the variation in the squeeze-out pressure against a molar amount of Hel 13-5 in the binary DPPG/Hel 13-5 preparation only. All of the preparations indicate hysteresis loops on cyclic π-*A* isotherms, where the loop size depends on DPPG contents in the surface films. Of interest, the large hysteresis was first detected for the cyclic ΔV-*A* isotherms in DPPG/Hel 13-5, not in DPPC/Hel 13-5 and DPPC/DPPG/Hel 13-5. The large hysteresis demonstrates that the mutual specific interaction triggers completely independent processes for Hel 13-5 during repeated compression and expansion processes: 1), squeezing-out into subsolution; and 2), close packing as a monolayer with DPPG at the interface. Judging from the new findings from AFM observations, the electrostatic interaction contributes to the aggregation of the squeezed-out Hel 13-5 molecules below the monolayers in lateral diameter under the compression process, and to their stabilization up to low surface pressures under the expansion process, which is special for the DPPG/Hel 13-5 system. This work systematically confirms the presence of specific interactions between the PG headgroup and the

polarized moiety of Hel 13-5. Furthermore, the results obtained using PS model systems will be helpful for understanding specific interactions between anionic phospholipids and native SP-B with regard to the physiological and biophysical functions of PS.

SUPPORTING MATERIAL

Figures are available at http://www.biophysj.org/biophysj/supplemental/S0006-3495(08)04007-1.

This work was supported by a Grant-in-Aid for Scientific Research (20500414) from the Japan Society for the Promotion of Science. This work was also supported by a Grant-in-Aid for Young Scientists 20810041 from JSPS (H.N.).

REFERENCES

1. Schürch, S., J. Goerke, and J. A. Clements. 1976. Direct determination of surface tension in the lung. *Proc. Natl. Acad. Sci. USA.* 73: 4698–4702.
2. Amrein, M., A. von Nahmen, and M. Sieber. 1997. A scanning force- and fluorescence light microscopy study of the structure and function of a model pulmonary surfactant. *Eur. Biophys. J.* 26:349–357.
3. Krol, S., M. Ross, M. Sieber, S. Kunneke, H.-J. Galla, et al. 2000. Formation of three-dimensional protein-lipid aggregates in monolayer films induced by surfactant protein B. *Biophys. J.* 79:904–918.
4. Takamoto, D. Y., M. M. Lipp, A. Von Nahmen, K. Y. C. Lee, A. J. Waring, et al. 2001. Interaction of lung surfactant proteins with anionic phospholipids. *Biophys. J.* 81:153–169.
5. Nakahara, H., S. Lee, G. Sugihara, and O. Shibata. 2006. Mode of interaction of hydrophobic amphiphilic α-helical peptide/dipalmitoylphosphatidylcholine with phosphatidylglycerol or palmitic acid at the air-water interface. *Langmuir.* 22:5792–5803.
6. Schürch, S., R. Qanbar, H. Bachofen, and F. Possmayer. 1995. The surface-associated surfactant reservoir in the alveolar lining. *Biol. Neonate.* 67 (Suppl 1):61–76.
7. Yu, S.-H., and F. Possmayer. 2003. Lipid compositional analysis of pulmonary surfactant monolayers and monolayer-associated reservoirs. *J. Lipid Res.* 44:621–629.
8. Krüger, P., J. E. Baatz, R. A. Dluhy, and M. Lösche. 2002. Effect of hydrophobic surfactant protein SP-C on binary phospholipid monolayers. Molecular machinery at the air/water interface. *Biophys. Chem.* 99:209–228.
9. Veldhuizen, R., K. Nag, S. Orgeig, and F. Possmayer. 1998. The role of lipids in pulmonary surfactant. *Biochim. Biophys. Acta.* 1408:90–108.
10. Clark, J. C., S. E. Wert, C. J. Bachurski, M. T. Stahlman, B. R. Stripp, et al. 1995. Targeted disruption of the surfactant protein B gene disrupts surfactant homeostasis, causing respiratory failure in newborn mice. *Proc. Natl. Acad. Sci. USA.* 92:7794–7798.
11. Nogee, L. M., G. Garnier, H. C. Dietz, L. Singer, A. M. Murphy, et al. 1994. A mutation in the surfactant protein B gene responsible for fatal neonatal respiratory disease in multiple kindreds. *J. Clin. Invest.* 93:1860–1863.
12. Ballard, P. L., L. M. Nogee, M. F. Beers, R. A. Ballard, B. C. Planer, et al. 1995. Partial deficiency of surfactant protein B in an infant with chronic lung disease. *Pediatrics.* 96:1046–1052.
13. Hawgood, S., B. J. Benson, J. Schilling, D. Damm, J. A. Clements, et al. 1987. Nucleotide and amino acid sequences of pulmonary surfactant protein SP 18 and evidence for cooperation between SP 18 and SP 28–36 in surfactant lipid adsorption. *Proc. Natl. Acad. Sci. USA.* 84:66–70.
14. Glasser, S. W., T. R. Korfhagen, T. Weaver, T. Pilot-Matias, J. L. Fox, et al. 1987. cDNA and deduced amino acid sequence of human pulmonary surfactant-associated proteolipid SPL(Phe). *Proc. Natl. Acad. Sci. USA.* 84:4007–4011.
15. Pérez-Gil, J., C. Casals, and D. Marsh. 1995. Interactions of hydrophobic lung surfactant proteins SP-B and SP-C with dipalmitoylphosphatidylcholine and dipalmitoylphosphatidylglycerol bilayers studied by electron spin resonance spectroscopy. *Biochemistry.* 34:3964–3971.
16. Revak, S. D., T. A. Merritt, C. G. Cochrane, G. P. Heldt, M. S. Alberts, et al. 1996. Efficacy of synthetic peptide-containing surfactant in the treatment of respiratory distress syndrome in preterm infant rhesus monkeys. *Pediatr. Res.* 39:715–724.
17. Ma, J., S. Koppenol, H. Yu, and G. Zografi. 1998. Effects of a cationic and hydrophobic peptide, KL4, on model lung surfactant lipid monolayers. *Biophys. J.* 74:1899–1907.
18. Wiswell, T. E., R. M. Smith, L. B. Katz, L. Mastroianni, D. Y. Wong, et al. 1999. Bronchopulmonary segmental lavage with Surfaxin (KL(4)-surfactant) for acute respiratory distress syndrome. *Am. J. Respir. Crit. Care Med.* 160:1188–1195.
19. Nakahara, H., S. Lee, G. Sugihara, C. -H. Chang, and O. Shibata. 2008. Langmuir monolayer of artificial pulmonary surfactant mixtures with an amphiphilic peptide at the air/water interface: comparison of new preparations with Surfacten (Surfactant TA). *Langmuir.* 24:3370–3379.
20. Nakahara, H., S. Nakamura, T. Hiranita, H. Kawasaki, S. Lee, et al. 2006. Mode of interaction of amphiphilicα-helical peptide with phosphatidylcholines at the air-water interface. *Langmuir.* 22:1182–1192.
21. Lee, S., T. Furuya, T. Kiyota, N. Takami, K. Murata, et al. 2001. De novo-designed peptide transforms Golgi-specific lipids into Golgi-like nanotubules. *J. Biol. Chem.* 276:41224–41228.
22. Kitamura, A., T. Kiyota, M. Tomohiro, A. Umeda, S. Lee, et al. 1999. Morphological behavior of acidic and neutral liposomes induced by basic amphiphilic α-helical peptides with systematically varied hydrophobic-hydrophilic balance. *Biophys. J.* 76:1457–1468.
23. Nakahara, H. 2008. Investigation and development of artificial lung surfactant preparations with a novel amphiphilic peptide for respiratory distress syndrome (RDS). PhD thesis. Kyushu Unversity, Fukuoka, Japan.
24. Tanaka, Y., T. Takei, T. Aiba, K. Masuda, A. Kiuchi, et al. 1986. Development of synthetic lung surfactants. *J. Lipid Res.* 27:475–485.
25. Lipp, M. M., K. Y. C. Lee, D. Y. Takamoto, J. A. Zasadzinski, and A. J. Waring. 1998. Coexistence of buckled and flat monolayers. *Phys. Rev. Lett.* 81:1650–1653.
26. Nahmen, A. V., M. Schenk, M. Sieber, and M. Amrein. 1997. The structure of a model pulmonary surfactant as revealed by scanning force microscopy. *Biophys. J.* 72:463–469.
27. Johansson, J. 1998. Structure and properties of surfactant protein C. *Biochim. Biophys. Acta.* 1408:161–172.
28. Robertson, B., and H. L. Halliday. 1998. Principles of surfactant replacement. *Biochim. Biophys. Acta.* 1408:346–361.
29. Serrano, A. G., and J. Pérez-Gil. 2006. Protein-lipid interactions and surface activity in the pulmonary surfactant system. *Chem. Phys. Lipids.* 141:105–118.
30. Breitenstein, D., J. J. Batenburg, B. Hagenhoff, and H. J. Galla. 2006. Lipid specificity of surfactant protein B studied by time-of-flight secondary ion mass spectrometry. *Biophys. J.* 91:1347–1356.
31. Seifert, M., D. Breitenstein, U. Klenz, M. C. Meyer, and H. J. Galla. 2007. Solubility versus electrostatics: what determines lipid/protein interaction in lung surfactant. *Biophys. J.* 93:1192–1203.
32. Diemel, R. V., M. M. E. Snel, A. J. Waring, F. J. Walther, L. M. G. van Golde, et al. 2002. Multilayer formation upon compression of surfactant monolayers depends on protein concentration as well as lipid composition. An atomic force microscopy study. *J. Biol. Chem.* 277:21179–21188.
33. Cruz, A., L. Vazquez, M. Velez, and J. Perez-Gil. 2004. Effect of pulmonary surfactant protein SP-B on the micro- and nanostructure of phospholipid films. *Biophys. J.* 86:308–320.
34. Bourdos, N., F. Kollmer, A. Benninghoven, M. Ross, M. Sieber, et al. 2000. Analysis of lung surfactant model systems with time-of-flight secondary ion mass spectrometry. *Biophys. J.* 79:357–369.

35. Morrow, M. R., S. Temple, J. Stewart, and K. M. Keough. 2007. Comparison of DPPC and DPPG environments in pulmonary surfactant models. *Biophys. J.* 93:164–175.

36. Kiyota, T., S. Lee, and G. Sugihara. 1996. Design and synthesis of amphiphilic α-helical model peptides with systematically varied hydrophobic-hydrophilic balance and their interaction with lipid- and biomembranes. *Biochemistry.* 35:13196–13204.

37. Sabatini, K., J. -P. Mattila, F. M. Megli, and P. K. J. Kinnuneny. 2006. Characterization of two oxidatively modified phospholipids in mixed monolayers with DPPC. *Biophys. J.* 90:4488–4499.

38. Ma, G., and H. C. Allen. 2007. Condensing effect of palmitic acid on DPPC in mixed Langmuir monolayers. *Langmuir.* 23:589–597.

39. Deleu, M., M. Paquot, P. Jacques, P. Thonart, Y. Adriaensen, et al. 1999. Nanometer scale organization of mixed surfactin/phosphatidylcholine monolayers. *Biophys. J.* 77:2304–2310.

40. Miller, C. E., D. D. Busath, B. Strongin, and J. Majewski. 2008. Integration of ganglioside GT_{1b} receptor into DPPE and DPPC phospholipid monolayers: an X-ray reflectivity and grazing-incidence diffraction study. *Biophys. J.* 95:3278–3286.

41. Miano, F., X. Zhao, J. R. Lu, and J. Penfold. 2007. Coadsorption of human milk lactoferrin into the dipalmitoylglycerolphosphatidylcholine phospholipid monolayer spread at the air/water interface. *Biophys. J.* 92:1254–1262.

42. Warriner, H. E., J. Ding, A. J. Waring, and J. A. Zasadzinski. 2002. A concentration-dependent mechanism by which serum albumin inactivates replacement lung surfactants. *Biophys. J.* 82:835–842.

43. Nakahara, H., O. Shibata, and Y. Moroi. 2005. Examination of surface adsorption of sodium chloride and sodium dodecyl sulfate by surface potential measurement at the air/solution interface. *Langmuir.* 21:9020–9022.

44. Nakahara, H., O. Shibata, M. Rusdi, and Y. Moroi. 2008. Examination of surface adsorption of soluble surfactants by surfacepotential measurement at the air/solution interface. *J. Phys. Chem. C.* 112:6398–6403.

45. Nakamura, S., H. Nakahara, M. P. Krafft, and O. Shibata. 2007. Two-component Langmuir monolayers of single-chain partially fluorinated amphiphiles with dipalmitoylphosphatidylcholine (DPPC). *Langmuir.* 23:12634–12644.

46. Koppenol, S., G. Zografi, and H. Yu. 1997. Mixing of saturated and unsaturated phosphatidylcholines and phosphatidylglycerols in monolayers at the air/water interface. *J. Colloid Interface Sci.* 189:158–166.

47. Grigoriev, D., R. Krustev, R. Miller, and U. Pison. 1999. Effect of monovalent ions on the monolayers phase behavior of the charged lipid DPPG. *J. Phys. Chem. B.* 103:1013–1018.

48. Petrov, J. G., E. E. Polymeropoulos, and H. Möhwald. 1996. On the three-capacitor model for surface potential of insoluble monolayers. *J. Phys. Chem.* 100:9860–9869.

49. Taylor, D. M., O. Novais de Oliveira, Jr., and H. Morgan. 1990. Models for interpreting surface potential measurements and their application to phospholipid monolayers. *J. Colloid Interface Sci.* 139:508–518.

50. Demchak, R. J., and T. Fort, Jr.. 1974. Surface dipole moments of close-packed nonionized monolayers at the air-water interface. *J. Colloid Interface Sci.* 46:191–202.

51. Shibata, O., and M. P. Krafft. 2000. Mixed Langmuir monolayers made from single-chain perfluoroalkylated amphiphiles. *Langmuir.* 16: 10281–10286.

52. Nakahara, H., S. Nakamura, H. Kawasaki, and O. Shibata. 2005. Properties of two-component Langmuir monolayer of single chain perfluorinated carboxylic acids with dipalmitoylphosphatidylcholine (DPPC). *Colloids Surf. B. Biointerfaces.* 41:285–298.

53. Joos, P., and R. A. Demel. 1969. The interaction energies of cholesterol and lecithin in spread mixed monolayers at the air-water interface. *Biochim. Biophys. Acta.* 183:447–457.

54. Matsumoto, Y., H. Nakahara, Y. Moroi, and O. Shibata. 2007. Langmuir monolayer properties of perfluorinated double long-chain salts with divalent counterions of separate electric charge at the air-water interface. *Langmuir.* 23:9629–9640.

55. Banerjee, R., and J. R. Bellare. 2001. Scoring of surface parameters of physiological relevance to surfactant therapy in respiratory distress syndrome. *J. Appl. Physiol.* 90:1447–1454.

56. Ivanova, T., I. Minkov, I. Panaiotov, P. Saulnier, and J. E. Proust. 2004. Dilatational properties and morphology of surface films spread from clinically used lung surfactants. *Colloid Polym. Sci.* 282:1258–1267.

57. Alonso, C., T. Alig, J. Yoon, F. Bringezu, H. Warriner, et al. 2004. More than a monolayer: relating lung surfactant structure and mechanics to composition. Biophys. J. 87:4188–4202.

58. Notter, R. H. 2000. Lung Surfactants: Basic Science and Clinical Applications. Marcel Dekker, New York, Basel.

59. Watkins, J. C. 1968. The surface properties of pure phospholipids in relation to those of lung extracts. *Biochim. Biophys. Acta.* 152:293–306.